

Magnonic Unidirectional Spin Hall Magnetoresistance in a Heavy-Metal–Ferromagnetic-Insulator Bilayer

G. Liu,^{1,§} Xi-guang Wang,^{2,§} Z. Z. Luan,¹ L. F. Zhou,¹ S. Y. Xia,¹ B. Yang,¹ Y. Z. Tian,¹
Guang-hua Guo,^{2,*} J. Du^{1,†} and D. Wu^{1,‡}

¹National Laboratory of Solid State Microstructures, Jiangsu Provincial Key Laboratory for Nanotechnology, Collaborative Innovation Center of Advanced Microstructures and Department of Physics, Nanjing University, Nanjing 210093, People's Republic of China

²School of Physics and Electronics, Central South University, Changsha 410083, People's Republic of China



(Received 7 June 2021; accepted 23 September 2021; published 12 November 2021)

We report the observation of the unidirectional spin Hall magnetoresistance (USMR), which depends on the current or magnetization direction, in heavy-metal–ferromagnetic-insulator bilayer, Pt-Y₃Fe₅O₁₂ (YIG). This USMR is apparently not caused by the mechanisms established in metallic bilayer, in which the ferromagnetic layer is required to be electrically conductive. From the magnetic field, current, temperature, and YIG thickness dependent measurements, the USMR is attributed to the asymmetric magnon creation and annihilation induced by the spin-orbit torque. This asymmetry and the resultant USMR are further revealed by the micromagnetic simulations combined with the spin-orbit torque and the spin drift-diffusion model. Our finding exhibits a nonlinear manipulation of magnons with the charge current.

DOI: 10.1103/PhysRevLett.127.207206

The heterostructures consisting of a heavy metal (HM) and a ferromagnet exhibit rich phenomena related to the spin current \mathbf{J}_s , such as spin-orbit torque (SOT) [1,2], spin Seebeck effect (SSE) [3–5], spin pumping [6–8], spin Hall magnetoresistance (SMR) [9–11] and unidirectional spin Hall magnetoresistance (USMR) [12–18]. In all these phenomena, the HM plays a critical role in interconverting between \mathbf{J}_s and the charge current \mathbf{J}_c via the spin Hall effect (SHE) and inverse spin Hall effect (ISHE) through its spin-orbit coupling. \mathbf{J}_s generated from an in-plane \mathbf{J}_c in the direction perpendicular to the sample plane is partially absorbed and/or reflected by the magnetic layer. The absorbed \mathbf{J}_s leads to the magnetization dynamics of the magnetic layer and even switching the magnetization \mathbf{M} [19–21]. The reflected \mathbf{J}_s can be converted into an additional \mathbf{J}_c via the ISHE to reduce the resistivity. Owing to the reflectivity of \mathbf{J}_s depending on the magnetization direction $\mathbf{m} = \mathbf{M}/M$, a magnetoresistance (MR), known as the SMR, appears.

Following the discoveries of the SMR, the recent progress still enriches the spin-current-induced MR effects in the HM-ferromagnet heterostructures such as the Rashba-Edelstein MR [22,23] and Hanle MR [24]. All these MR effects have a characteristic of the invariance under \mathbf{J}_c or \mathbf{m} reversal. In contrast, a newly discovered USMR is determined by the product $(\mathbf{J}_c \times \mathbf{m} \cdot \hat{\mathbf{z}})$, where $\hat{\mathbf{z}}$ is the unit vector perpendicular to the layer plane, meaning that the USMR is odd under \mathbf{J}_c or \mathbf{m} reversal [12]. So far, two mechanisms were proposed to explain the USMR [14,25]. One is the interface and bulk spin-dependent scatterings. The scattering rate or the electron transmission

probability at the HM-ferromagnet interface depends on the orientation of the spin polarization σ of \mathbf{J}_s in the HM relative to \mathbf{m} , resulting in an interfacial origin USMR. Owing to the spin-dependent conductivity in the ferromagnet, the injected spins from the HM into the ferromagnet bring about a spin accumulation inside the ferromagnet, leading to a change of the ferromagnetic layer conductivity. This mechanism is in analogy to the giant magnetoresistance [26,27]. The other one is the electron-magnon scattering. Magnons are created (or annihilated) in the ferromagnet by absorbing \mathbf{J}_s [28]. As a result, the strength of the electron-magnon scattering and the corresponding resistance of the ferromagnetic layer are altered, and the USMR emerges accordingly.

It is essential to observe the USMR that the ferromagnetic layer is electrically conductive according to the above proposed mechanisms [14–17]. If the ferromagnetic metal is replaced with a ferromagnetic insulator (FMI), all electrons must be scattered back to the HM layer at the interface, meaning that the interface scattering is not spin dependent and hence the interface spin scattering mechanism fails. For the FMI, the electrical insulator property cannot be altered by the injected spins and the spin-current-modulated magnon population, implying that the bulk spin-dependent and electron-magnon scattering mechanisms are not applicable any more. In other words, the USMR cannot occur in the HM-FMI heterostructures according to the above mechanisms.

However, recent theoretical calculations predict a magnonic USMR stemming from the asymmetric magnon creation and annihilation in the FMI layer [29,30].

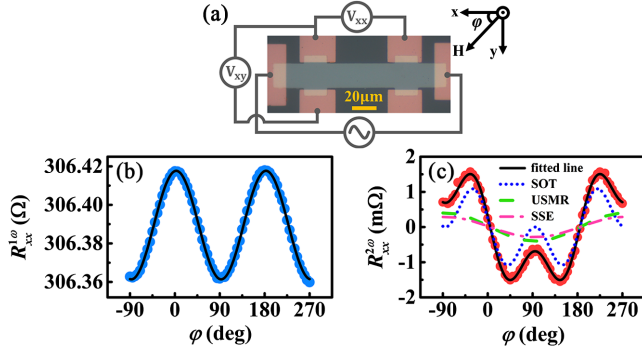


FIG. 1. (a) Optical micrograph of the sample Pt-YIG and the setup of MR and Hall resistance measurements. The current is injected along the x direction and H is applied in the xy plane. Angular dependences of $R_{xx}^{1\omega}$ (b) and $R_{xx}^{2\omega}$ (c) measured at 307.4 K, 20 Oe, and $j_0 = 6.7 \times 10^{10}$ A/m². The solid line is the fit to $\cos^2\varphi$ in Fig. 1(b). The green dashed, pink dot-dashed, and blue dotted lines in Fig. 1(c) are the fitted components contributed by the USMR, SSE, and SOT, respectively. The solid line is the sum of those three contributions.

An experimental evidence of this effect is still absent. Here, we report the demonstration of the magnonic USMR in Pt-Y₃Fe₅O₁₂ (YIG) bilayers. This USMR is sensitive to magnetic field and temperature, and disappears at high field ($> \sim 1000$ Oe) and low temperature ($< \sim 100$ K), suggesting the origin related with magnons. The USMR monotonically increases with increasing J_c or decreasing the YIG thickness t_{YIG} , reflecting the important role of the SHE and the corresponding SOT strength. Our observation is explained by the alteration of the spin current reflectivity associated with an asymmetric change in the magnon creation and annihilation, while σ is switched from antiparallel to parallel to \mathbf{m} . This mechanism is further confirmed by the numerical simulations combining the Landau-Lifshitz-Gilbert (LLG) equation with the spin drift-diffusion model.

The sample used in this work is Pt(3 nm)-YIG(9.7 nm), unless otherwise stated. The YIG films were grown on Gd₃Ga₅O₁₂ (GGG) (111) substrate by pulsed laser deposition (PLD). During the deposition, the substrates were heated to 730 °C in an oxygen atmosphere of 0.07 torr and the KrF excimer laser was applied at a repetition of 4 Hz with the energy density 150 mJ/mm². The YIG films show the saturation field less than ~ 4 Oe [31]. Two ultraviolet lithography steps were adopted to pattern a Pt Hall-bar and 15-nm-thick Au bonding pads, followed by dc magnetron sputtering the metallic films and the lift-off procedure. Before deposition, Ar⁺ plasma was applied to remove the possible residual photoresist to obtain clean interface. The optical micrograph of the sample and measurement setup are depicted in Fig. 1(a). The width w and length l (between the center of two Hall arms) of the Hall bar are 19.5 and 81.5 μm , respectively. The magnetotransport measurements were carried out in a Quantum Design PPMS using

a Keithley 6221 source meter and a Stanford SR865A lock-in amplifier.

We applied an ac current $j = j_0 \sin \omega t$ with frequency $\omega/2\pi = 7$ Hz along the x direction and a magnetic field H in the sample plane, as shown in Fig. 1(a). Then, the first and second harmonic longitudinal resistances ($R_{xx}^{1\omega}$ and $R_{xx}^{2\omega}$) and Hall resistances ($R_{xy}^{1\omega}$ and $R_{xy}^{2\omega}$) were measured with the sample rotated in the xy plane under a constant H . Here, $R_{xx}^{1\omega}$ and $R_{xy}^{1\omega}$ represent the conventional current-independent resistance and Hall resistance, respectively, whereas $R_{xx}^{2\omega}$ represents the nonlinear signal which depends on the current direction and amplitude [12]. Since a relatively large current is applied to improve the signal-to-noise ratio, the Pt-film temperature T significantly increases due to the Joule heating, up to $\Delta T = 7.4$ K at $j_0 = 6.7 \times 10^{10}$ A/m². To overcome this drawback, the T -dependent resistance of the Pt-Hall-bar is measured using a small current density ($j_0 = 1.7 \times 10^9$ A/m²). Then T is accurately determined via the T -dependent resistance in all measurements.

Figures 1(b) and 1(c) show $R_{xx}^{1\omega}$ and $R_{xx}^{2\omega}$ as a function of φ measured at 307.4 K and $j_0 = 6.7 \times 10^{10}$ A/m² for Pt-YIG, where φ is the angle between \mathbf{H} and the x axis. The applied field is set at 20 Oe, which is large enough to make \mathbf{M} align with \mathbf{H} . $R_{xx}^{1\omega}$ exhibits a typical SMR behavior, following a $\cos^2\varphi$ function [solid line in Fig. 1(b) for fitting] [9], with the SMR ratio $\xi_{\text{SMR}} = \Delta R_{xx}^{1\omega} / R_{xx}^{1\omega}(0^\circ) = [R_{xx}^{1\omega}(0^\circ) - R_{xx}^{1\omega}(90^\circ)] / R_{xx}^{1\omega}(0^\circ) = 0.019\%$. $R_{xx}^{1\omega}$ and ξ_{SMR} are almost constant with varying j_0 and H [31].

The applied current density is large enough to generate the SOT to give rise to the \mathbf{M} precession, meaning that the direction of \mathbf{M} oscillates with respect to the x axis [38,39]. As a result, the time-averaged SMR is nonlinearly modulated, leading to the second harmonic signals. For the HM-ferromagnet heterostructures with a negligible in-plane anisotropy, the SOT-induced $R_{xx}^{2\omega}$ is given by [39]

$$R_{xx}^{\text{SOT}} = -2\Delta R_{xx}^{1\omega}(H_{\text{FL}} + H_{\text{Oe}}) \sin\varphi \cos^2\varphi / H, \quad (1)$$

where H_{FL} and H_{Oe} are the effective fields of the fieldlike torque and the Oersted field, respectively. Indeed, the curve of $R_{xx}^{2\omega}(\varphi)$ exhibits the distinct characteristics of a $\sin\varphi \cos^2\varphi$ behavior. To quantitatively evaluate the contribution of the SOT to $R_{xx}^{2\omega}$, we carried out the angular dependent $R_{xx}^{2\omega}$ measurements at various H , shown in Fig. 2(a). The component of $\sin\varphi \cos^2\varphi$ is obviously and steadily reduced with increasing H , consistent with the expectation from Eq. (1). Eventually, only a sinusoidal behavior is observed at the relatively high field, which is the unidirectional MR (UMR) including several contributions. Thus, we fit $R_{xx}^{2\omega}(\varphi)$ with two terms, $R_{xx}^{2\omega} = R_{xx}^{\text{SOT}} + R_{xx}^{\text{UMR}} \sin\varphi$, where R_{xx}^{UMR} is the UMR and will be discussed later. We find that the fittings [solid lines in Fig. 2(a)] perfectly match the experimental data. The fitted

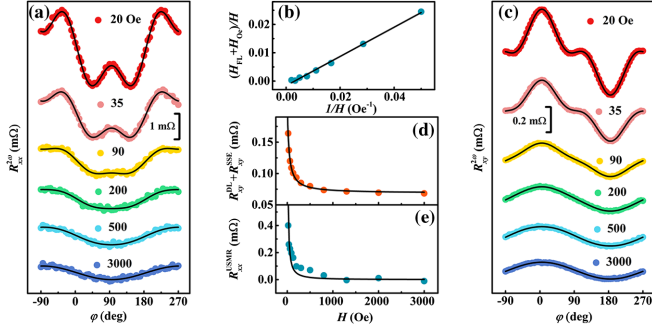


FIG. 2. Angular dependences of $R_{xx}^{2\omega}$ (a) and $R_{xy}^{2\omega}$ (c) measured at different H with $T = 307.4$ K and $j_0 = 6.7 \times 10^{10}$ A/m². The solid lines are the fittings described in the text. (b) The extracted $(H_{\text{FL}} + H_{\text{Oe}})/H$ from the fitting in Fig. 2(a) as a function of $1/H$. The solid line is the linear fit. (d) Field dependence of $R_{xy}^{\text{DL}} + R_{xy}^{\text{SSE}}$. The solid line is the fit using Eq. (3). (e) Field dependence of the USMR and the theoretical simulation results (solid line).

values of $(H_{\text{FL}} + H_{\text{Oe}})/H$ at different H exhibit a linear dependence on $1/H$, as shown in Fig. 2(b), confirming the contribution of the SOT to $R_{xx}^{2\omega}$ [39,40].

Next, we investigated the origins of R_{xx}^{UMR} . Considering that the current flows only in Pt and YIG has much poorer thermal conductivity than Pt, the temperature gradient perpendicular to the film plane induced by the Joule heating is expected to be much larger than the metallic system. The Joule heating power reads $j^2 = j_0^2 \sin^2 \omega t \sim \cos 2\omega t$, indicating that the temperature gradient and the associated magnetothermal effects including the anomalous Nernst effect (ANE) [41,42] and the SSE [43] must have contributions to $R_{xx}^{2\omega}$. Since YIG is a FMI, the ANE can be immediately ruled out. To estimate the SSE contribution R_{xx}^{SSE} to R_{xx}^{UMR} , the angular dependent $R_{xy}^{2\omega}$ was measured at different H , shown in Fig. 2(c). $R_{xy}^{2\omega}$ originating from the SSE and SOT can be described by [38]

$$R_{xy}^{2\omega} = (R_{xy}^{\text{DL}} + R_{xy}^{\text{SSE}}) \cos \varphi + R_{xy}^{\text{FL}}(2\cos^3 \varphi - \cos \varphi), \quad (2)$$

with

$$\begin{aligned} R_{xy}^{\text{DL}} &= R_{\text{AHE}} H_{\text{DL}} / (H_{\text{eff}} + H) \quad \text{and} \\ R_{xy}^{\text{FL}} &= 2R_{\text{PHE}} (H_{\text{FL}} + H_{\text{Oe}}) / H, \end{aligned} \quad (3)$$

where R_{xy}^{SSE} is the contribution of the SSE to the transverse signal, R_{AHE} and R_{PHE} are the anomalous Hall and planar Hall resistance, respectively, H_{DL} and H_{eff} are the effective fields of the dampinglike SOT and the out-of-plane anisotropy, respectively. The experimental $R_{xy}^{2\omega}(\varphi)$ can be fitted by Eq. (2) very well [solid lines in Fig. 2(c)]. The obtained coefficient $R_{xy}^{\text{DL}} + R_{xy}^{\text{SSE}}$ can be fitted using Eq. (3), as the solid line shown in Fig. 2(d). R_{xy}^{SSE} is considered to be independent of H because of the small field range

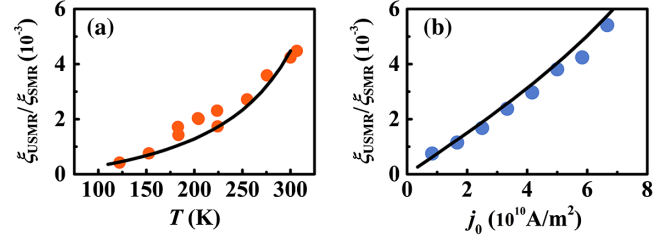


FIG. 3. (a) Temperature dependence of $\xi_{\text{USMR}}/\xi_{\text{SSMR}}$ measured at $j_0 = 5.8 \times 10^{10}$ A/m² and 35 Oe. (b) Current dependence of $\xi_{\text{USMR}}/\xi_{\text{SSMR}}$ measured at 300 K and 35 Oe. The solid lines are the theoretical simulation results.

(≤ 3000 Oe) and ultrathin YIG film [31,44,45]. The fitting yields $R_{xy}^{\text{SSE}} = 0.069$ m Ω . The SSE-induced UMR R_{xx}^{SSE} is, then, calculated by the length-to-width ratio of the Hall bar, $R_{xx}^{\text{SSE}} = R_{xy}^{\text{SSE}} l/w = 0.290$ m Ω [pink dot-dashed line in Fig. 1(c)]. Furthermore, R_{xx}^{SSE} is found to be linearly dependent on j_0 , confirming R_{xx}^{SSE} stemmed from the SSE [31]. R_{xx}^{SSE} is also determined to be ~ 0.290 m Ω from the constant term in $R_{xx}^{\text{UMR}}(H)$, confirming the validity of the estimated R_{xx}^{SSE} [31]. We find that R_{xx}^{SSE} only amounts to part of R_{xx}^{UMR} , e.g., $R_{xx}^{\text{SSE}}/R_{xx}^{\text{UMR}} \approx 42.0\%$ at 20 Oe. Since this additional MR, $R_{xx}^{\text{USMR}} (= R_{xx}^{\text{UMR}} - R_{xx}^{\text{SSE}})$, depends on the direction of \mathbf{m} and Pt is the only conducting layer, it should originate from \mathbf{J}_s . Therefore, we ascribe R_{xx}^{USMR} to the USMR [green dashed line in Fig. 1(c)]. The USMR ratio, $\xi_{\text{USMR}} = R_{xx}^{\text{USMR}}/R_{xx}^{1\omega}$, is about 1.3×10^{-6} at 20 Oe, 2 orders of magnitude smaller than ξ_{SSMR} .

Figure 2(e) shows R_{xx}^{USMR} extracted from Fig. 2(a) as a function of H . The USMR rapidly decreases with increasing H and vanishes above ~ 1000 Oe. The USMR caused by the bulk and interface spin-dependent scatterings is independent of H , meaning a constant USMR value at high field. Our result further rules out the spin-dependent scattering mechanisms. On the other hand, the similar behavior of the signal suppression is observed in the SSE in Pt-YIG and the USMR in Pt-Co [14,44], both of which are ascribed to the reduction of the magnon population by the magnon gap opening caused by the Zeeman effect. This provides us with an important clue that our observed USMR in Pt-YIG should be correlated with the magnon creation and annihilation.

The nonlocal measurements reveal that the thermal fluctuation is essential for the spin-current-induced magnon creation and annihilation [46,47]. The dependence of the normalized USMR ratio $\xi_{\text{USMR}}/\xi_{\text{SSMR}}$ on T measured at $j_0 = 5.8 \times 10^{10}$ A/m² and 35 Oe is shown in Fig. 3(a). The USMR monotonically decreases with decreasing T and almost vanishes at ~ 100 K. This result shows much stronger temperature dependence than that in the metallic system [14], highlighting again that magnons play a decisive role and the spin-dependent scattering is unrelated to our observations. Otherwise, a finite USMR should be

present at low T . Figure 3(b) shows $\xi_{\text{USMR}}/\xi_{\text{SMR}}$ as a function of j_0 at 300 K and 35 Oe. Note that T (or $R_{xx}^{1\omega}$) is simultaneously controlled by the PPMS temperature controller to remain unchanged while varying j_0 . R_{xx}^{USMR} increases with increasing j_0 , reflecting that R_{xx}^{USMR} is a nonlinear effect on j_0 and related to the SHE.

As discussed above, the mechanisms established on the metallic systems cannot explain our observations. The SHE-generated \mathbf{J}_s is completely reflected while $\boldsymbol{\sigma}$ and \mathbf{m} are collinear according to the SMR mechanism, meaning the minimum resistance [48]. In fact, \mathbf{J}_s can exert the SOT to \mathbf{M} to create (or annihilate) magnons in the FMI under this condition owing to the thermal fluctuation, which was demonstrated in the magnon transport devices in the in-plane [49] and out-of-plane nonlocal geometries [50,51]. This effect could open up a new channel to absorb \mathbf{J}_s by the FMI in addition to the coherent precession, resulting in diminishing the reflected \mathbf{J}_s and hence the ISHE-converted charge current, in analogy to the SMR. To quantitatively understand the influence of this effect on resistance, we carried out numerical simulation based on the LLG equation including the SOT $\boldsymbol{\tau}_{\text{SOT}}$ [29],

$$\frac{d\mathbf{m}}{dt} = -\gamma\mathbf{m} \times [\mathbf{H}_{\text{eff}} + \mathbf{h}_t(T)] + \alpha\mathbf{m} \times \frac{d\mathbf{m}}{dt} + \boldsymbol{\tau}_{\text{SOT}}, \quad (4)$$

and the spin drift-diffusion model. Here, γ is the gyromagnetic ratio, \mathbf{H}_{eff} is the effective field, α is the Gilbert damping factor, and $\boldsymbol{\tau}_{\text{SOT}}$ is given by $\boldsymbol{\tau}_{\text{SOT}} = c j / (M_s t_{\text{YIG}}) (\mathbf{m} \times \boldsymbol{\sigma} \times \mathbf{m})$, where M_s is the saturation magnetization and the coefficient c is a constant for a given t_{YIG} . Owing to the thermal random magnetic field $\mathbf{h}_t(T)$, the SOT is nonzero and exerted to \mathbf{m} to modulate the magnetic fluctuations (or magnon numbers) even for $\boldsymbol{\sigma} \parallel \mathbf{m}$ [21]. The simulation indeed shows that \mathbf{J}_s in Pt is converted into a magnonic spin current in YIG partially through creating (annihilating) magnons at the interface for $\boldsymbol{\sigma} \parallel \mathbf{m}$, as shown in Supplemental Material [31], effectively resulting in the slight deviation of the collinear alignment between $\boldsymbol{\sigma}$ and \mathbf{m} . Importantly, the magnon creation is more efficient than the magnon annihilation due to the nonlinearity of the LLG equation to current [29], as schematically shown in Figs. 4(a) and 4(b), meaning that the deviation angle in the antiparallel configuration is larger than that in the parallel configuration. Consequently, the reflected \mathbf{J}_s and the corresponding ISHE-converted charge current are unequal for the opposite \mathbf{J}_c direction, giving rise to the USMR [31].

We simulated the magnonic USMR at different H , as shown the solid line in Fig. 2(e), in good agreement with the experimental values. The magnon number difference between $\varphi = \pi/2$ and $\varphi = 3\pi/2$ shows the same trend with the USMR [31], confirming the USMR originating from the asymmetric magnon creation and annihilation. The rapid decrease of the magnonic USMR below ~ 1000 Oe suggests that the low-frequency magnons of which the

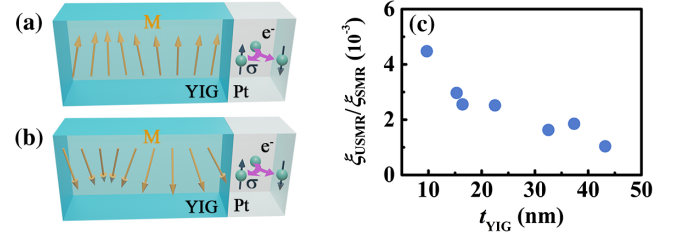


FIG. 4. Schematics of the magnon annihilation (a) and creation (b) by the SOT in Pt-YIG. (c) YIG thickness dependence of the USMR measured at 306 K, 35 Oe, and $j_0 = 5.8 \times 10^{10}$ A/m².

energy is less than the Zeeman energy at ~ 1000 Oe provide a dominant contribution to the USMR. In contrast, the SSE signal in Pt-YIG is gradually suppressed with increasing H and showing nonsaturation for field up to 90 kOe for thick YIG film and almost constant for thin YIG film ($< \sim 300$ nm) [45]. Therefore, the H -dependent measurements provide a simple approach to distinguish the magnonic USMR from the SSE. The magnon creation and annihilation also result in the USMR in metallic systems with similar H dependence [14,17]. This part of the USMR stems from the electron-magnon scattering in the ferromagnetic metallic layer, meaning the bulk contribution. ξ_{USMR} is estimated to be as large as $\sim 10^{-5}$ in Pt-Co at $j_0 = 6.7 \times 10^{10}$ A/m², 300 K and 300 Oe from the previous reports [14], in comparison with $\sim 10^{-7}$ in Pt-YIG under the similar conditions. The mechanism that we proposed could be present in metallic systems. However, because of the similar behavior and very small magnitude, it is difficult to distinguish this mechanism from the electron-magnon scattering.

To verify the above theory further, the T - and j_0 -dependent R_{xx}^{USMR} are simulated, as shown the solid lines in Figs. 3(a) and 3(b), respectively. The good agreements confirm the validity of our theoretical model. The magnon creation and annihilation are more pronounced at high temperature [29,30,46], leading to the enhanced asymmetric creation and annihilation and USMR. We note that the j_0 -dependent result is weakly nonlinear, revealing that the created magnon number increases more than the annihilated magnon number with increasing j_0 .

According to $\boldsymbol{\tau}_{\text{SOT}} \propto 1/t_{\text{YIG}}$, t_{YIG} could influence the SOT strength and thereby the magnonic USMR. Finally, we further prove the robustness of the magnonic USMR by changing t_{YIG} . Figure 4(c) shows $\xi_{\text{USMR}}/\xi_{\text{SMR}}$ as a function of t_{YIG} extracted from the angular dependent $R_{xx}^{1\omega}$, $R_{xx}^{2\omega}$, and $R_{xy}^{2\omega}$ measurements performed at $j_0 = 5.8 \times 10^{10}$ A/m², 35 Oe, and 306 K. As expected, the USMR ratio monotonically decreases with increasing t_{YIG} . This behavior is in sharp contrast to the nonmonotonic behavior of the USMR in Pt-Co, which peaks at a Co thickness of 10 nm owing to the USMR governed by the spin diffusion in Co [18]. We note that the USMR is also predicted by considering the interfacial spin current in terms of the spin mixing

conductance [30]. $\xi_{\text{USMR}}/\xi_{\text{SMR}}$ is expected to increase with increasing t_{YIG} for thin YIG in this model, opposite to our observation. Our result explains no USMR observed in Pt-YIG in the previous report, in which t_{YIG} is 90 nm [13]. The USMR ratio of Pt(3 nm)-YIG(90 nm) is extrapolated to be $10^{-8} \sim 10^{-9}$ from our results, well below the experimental resolution.

In conclusion, we experimentally demonstrate the USMR in Pt-YIG, which is unexpected based on the established USMR mechanisms. The USMR is attributed to the simultaneous action of the nonlinear absorption of the SHE-generated spin current and the ISHE. The USMR ratio can be controlled by the external magnetic field, temperature, charge current density, and YIG film thickness. Our finding reveals a new mechanism for the USMR and opens up a door to nonlinearly manipulate magnons for the magnon-based logic devices.

This work was supported by National Natural Science Foundation of China (52025012, 11727808, 51971109, 11704415, 12074437 and 12174452) and National Key R&D Program of China (2017YFA0303202).

*Corresponding author.
guogh@csu.edu.cn

†Corresponding author.
jdu@nju.edu.cn

‡Corresponding author.
dwu@nju.edu.cn

§These authors contributed equally to this work.

- [1] K. Garello, I. M. Miron, C. O. Avci, F. Freimuth, Y. Mokrousov, S. Blügel, S. Auffret, O. Boulle, G. Gaudin, and P. Gambardella, Symmetry and magnitude of spin-orbit torques in ferromagnetic heterostructures, *Nat. Nanotechnol.* **8**, 587 (2013).
- [2] A. Manchon, J. Železný, I. M. Miron, T. Jungwirth, J. Sinova, A. Thiaville, K. Garello, and P. Gambardella, Current-induced spin-orbit torques in ferromagnetic and antiferromagnetic systems, *Rev. Mod. Phys.* **91**, 035004 (2019).
- [3] K. Uchida, H. Adachi, T. Ota, H. Nakayama, S. Maekawa, and E. Saitoh, Observation of longitudinal spin-Seebeck effect in magnetic insulators, *Appl. Phys. Lett.* **97**, 172505 (2010).
- [4] D. Qu, S. Y. Huang, J. Hu, R. Wu, and C. L. Chien, Intrinsic Spin Seebeck Effect in Au/YIG, *Phys. Rev. Lett.* **110**, 067206 (2013).
- [5] B. Yang, S. Y. Xia, H. Zhao, G. Liu, J. Du, K. Shen, Z. Qiu, and D. Wu, Revealing thermally driven distortion of magnon dispersion by spin Seebeck effect in $\text{Gd}_3\text{Fe}_5\text{O}_{12}$, *Phys. Rev. B* **103**, 054411 (2021).
- [6] Y. Tserkovnyak, A. Brataas, and G. E. W. Bauer, Spin pumping and magnetization dynamics in metallic multilayers, *Phys. Rev. B* **66**, 224403 (2002).
- [7] E. Saitoh, M. Ueda, H. Miyajima, and G. Tatara, Conversion of spin current into charge current at room temperature: Inverse spin-Hall effect, *Appl. Phys. Lett.* **88**, 182509 (2006).
- [8] O. Mosendz, J. E. Pearson, F. Y. Fradin, G. E. W. Bauer, S. D. Bader, and A. Hoffmann, Quantifying Spin Hall Angles from Spin Pumping: Experiments and Theory, *Phys. Rev. Lett.* **104**, 046601 (2010).
- [9] H. Nakayama, M. Althammer, Y.-T. Chen, K. Uchida, Y. Kajiwara, D. Kikuchi, T. Ohtani, S. Geprägs, M. Opel, S. Takahashi, R. Gross, G. E. W. Bauer, S. T. B. Goennenwein, and E. Saitoh, Spin Hall Magnetoresistance Induced by a Nonequilibrium Proximity Effect, *Phys. Rev. Lett.* **110**, 206601 (2013).
- [10] J. Kim, P. Sheng, S. Takahashi, S. Mitani, and M. Hayashi, Spin Hall Magnetoresistance in Metallic Bilayers, *Phys. Rev. Lett.* **116**, 097201 (2016).
- [11] C. Hahn, G. de Loubens, O. Klein, M. Viret, V. V. Naletov, and J. Ben Youssef, Comparative measurements of inverse spin Hall effects and magnetoresistance in YIG/Pt and YIG/Ta, *Phys. Rev. B* **87**, 174417 (2013).
- [12] C. O. Avci, K. Garello, A. Ghosh, M. Gabureac, S. F. Alvarado, and P. Gambardella, Unidirectional spin Hall magnetoresistance in ferromagnet/normal metal bilayers, *Nat. Phys.* **11**, 570 (2015).
- [13] C. O. Avci, K. Garello, J. Mendil, A. Ghosh, N. Blasakis, M. Gabureac, M. Trassin, M. Fiebig, and P. Gambardella, Magnetoresistance of heavy and light metal/ferromagnet bilayers, *Appl. Phys. Lett.* **107**, 192405 (2015).
- [14] C. O. Avci, J. Mendil, G. S. D. Beach, and P. Gambardella, Origins of the Unidirectional Spin Hall Magnetoresistance in Metallic Bilayers, *Phys. Rev. Lett.* **121**, 087207 (2018).
- [15] I. V. Borisenko, V. E. Demidov, S. Urazhdin, A. B. Rinkevich, and S. O. Demokritov, Relation between unidirectional spin Hall magnetoresistance and spin current-driven magnon generation, *Appl. Phys. Lett.* **113**, 062403 (2018).
- [16] K. Hasegawa, T. Koyama, and D. Chiba, Enhanced unidirectional spin Hall magnetoresistance in a Pt/Co system with a Cu interlayer, *Phys. Rev. B* **103**, L020411 (2021).
- [17] T. Li, S. Kim, S.-J. Lee, S.-W. Lee, T. Koyama, D. Chiba, T. Moriyama, K.-J. Lee, K.-J. Kim, and T. Ono, Origin of threshold current density for asymmetric magnetoresistance in Pt/Py bilayers, *Appl. Phys. Express* **10**, 073001 (2017).
- [18] Y. Yin, D.-S. Han, M. C. H. de Jong, R. Lavrijsen, R. A. Duine, H. J. M. Swagten, and B. Koopmans, Thickness dependence of unidirectional spin-Hall magnetoresistance in metallic bilayers, *Appl. Phys. Lett.* **111**, 232405 (2017).
- [19] L. Liu, O. J. Lee, T. J. Gudmundsen, D. C. Ralph, and R. A. Buhrman, Current-Induced Switching of Perpendicularly Magnetized Magnetic Layers Using Spin Torque from the Spin Hall Effect, *Phys. Rev. Lett.* **109**, 096602 (2012).
- [20] S. S.-L. Zhang and S. Zhang, Spin convertance at magnetic interfaces, *Phys. Rev. B* **86**, 214424 (2012).
- [21] V. E. Demidov, S. Urazhdin, E. R. J. Edwards, M. D. Stiles, R. D. McMichael, and S. O. Demokritov, Control of Magnetic Fluctuations by Spin Current, *Phys. Rev. Lett.* **107**, 107204 (2011).
- [22] H. Nakayama, Y. Kanno, H. An, T. Tashiro, S. Haku, A. Nomura, and K. Ando, Rashba-Edelstein Magnetoresistance in Metallic Heterostructures, *Phys. Rev. Lett.* **117**, 116602 (2016).

- [23] J. Kim, Y.-T. Chen, S. Karube, S. Takahashi, K. Kondou, G. Tatara, and Y. Otani, Evaluation of bulk-interface contributions to Edelstein magnetoresistance at metal/oxide interfaces, *Phys. Rev. B* **96**, 140409(R) (2017).
- [24] S. Vélez, V.N. Golovach, A. Bedoya-Pinto, M. Isasa, E. Sagasta, M. Abadia, C. Rogero, L. E. Hueso, F. S. Bergeret, and F. Casanova, Hanle Magnetoresistance in Thin Metal Films with Strong Spin-Orbit Coupling, *Phys. Rev. Lett.* **116**, 016603 (2016).
- [25] S. S.-L. Zhang and G. Vignale, Theory of unidirectional spin Hall magnetoresistance in heavy-metal/ferromagnetic-metal bilayers, *Phys. Rev. B* **94**, 140411(R) (2016).
- [26] M. N. Baibich, J. M. Broto, A. Fert, F. N. Van Dau, F. Petroff, P. Etienne, G. Creuzet, A. Friederich, and J. Chazelas, Giant Magnetoresistance of (001)Fe/(001)Cr Magnetic Superlattices, *Phys. Rev. Lett.* **61**, 2472 (1988).
- [27] G. Binasch, P. Grinberg, F. Saurenbach, and W. Zinn, Enhanced magnetoresistance in layered magnetic structures with antiferromagnetic interlayer exchange, *Phys. Rev. B* **39**, 4828(R) (1989).
- [28] B. Raquet, M. Viret, E. Sondergard, O. Cespedes, and R. Mamy, Electron-magnon scattering and magnetic resistivity in 3d ferromagnets, *Phys. Rev. B* **66**, 024433 (2002).
- [29] X. Wang, Z. Zhou, Y. Nie, Q. Xia, and G. Guo, Self-consistent study of local and nonlocal magnetoresistance in a YIG/Pt bilayer, *Phys. Rev. B* **97**, 094401 (2018).
- [30] W. P. Sterk, D. Peerlings, and R. A. Duine, Magnon contribution to unidirectional spin Hall magnetoresistance in ferromagnetic-insulator/heavy-metal bilayers, *Phys. Rev. B* **99**, 064438 (2019).
- [31] See Supplemental Material at <http://link.aps.org/supplemental/10.1103/PhysRevLett.127.207206> for a description of the properties of the YIG film, magnetoresistance and SSE in Pt/YIG, and theoretical simulations, which includes Refs. [32–37].
- [32] M. C. Onbasli, A. Kehlberger, D. H. Kim, G. Jakob, M. Kläui, A. V. Chumak, B. Hillebrands, and C. A. Ross, Pulsed laser deposition of epitaxial yttrium iron garnet films with low Gilbert damping and bulk-like magnetization, *APL Mater.* **2**, 106102 (2014).
- [33] V. Cherepanov, I. Kolokolov, and V. L'vov, The saga of YIG: Spectra, thermodynamics, interaction and relaxation of magnons in a complex magnet, *Phys. Rep.* **229**, 81 (1993).
- [34] S. R. Marmion, M. Ali, M. McLaren, D. A. Williams, and B. J. Hickey, Temperature dependence of spin Hall magnetoresistance in thin YIG/Pt films, *Phys. Rev. B* **89**, 220404(R) (2014).
- [35] M. Isasa, E. Villamor, L. E. Hueso, M. Gradhand, and F. Casanova, Temperature dependence of spin diffusion length and spin Hall angle in Au and Pt, *Phys. Rev. B* **91**, 024402 (2015).
- [36] J. Sinova, S. O. Valenzuela, J. Wunderlich, C. H. Back, and T. Jungwirth, Spin Hall effects, *Rev. Mod. Phys.* **87**, 1213 (2015).
- [37] M. Haertinger, C. H. Back, J. Lotze, M. Weiler, S. Geprägs, H. Huebl, S. T. B. Goennenwein, and G. Woltersdorf, Spin pumping in YIG/Pt bilayers as a function of layer thickness, *Phys. Rev. B* **92**, 054437 (2015).
- [38] C. O. Avci, K. Garello, M. Gabureac, A. Ghosh, A. Fuhrer, S. F. Alvarado, and P. Gambardella, Interplay of spin-orbit torque and thermoelectric effects in ferromagnet/normal-metal bilayers, *Phys. Rev. B* **90**, 224427 (2014).
- [39] B. Han, B. Wang, Z. Yan, T. Wang, D. Yang, X. Fan, Y. Wang, and J. Cao, Determination of the Spin-Orbit Torques in Ferromagnetic–Heavy-Metal Bilayers Using Harmonic Longitudinal Voltage Measurements, *Phys. Rev. Applied* **13**, 014065 (2020).
- [40] Y. Chen, D. Roy, E. Cogulu, H. Chang, M. Wu, and A. D. Kent, First harmonic measurements of the spin Seebeck effect, *Appl. Phys. Lett.* **113**, 202403 (2018).
- [41] T. C. Chuang, P. L. Su, P. H. Wu, and S. Y. Huang, Enhancement of the anomalous Nernst effect in ferromagnetic thin films, *Phys. Rev. B* **96**, 174406 (2017).
- [42] T. Kikkawa, K. Uchida, S. Daimon, Y. Shiomi, H. Adachi, Z. Qiu, D. Hou, X.-F. Jin, S. Maekawa, and E. Saitoh, Separation of longitudinal spin Seebeck effect from anomalous Nernst effect: Determination of origin of transverse thermoelectric voltage in metal/insulator junctions, *Phys. Rev. B* **88**, 214403 (2013).
- [43] N. Vlietstra, J. Shan, B. J. van Wees, M. Isasa, F. Casanova, and J. Ben Youssef, Simultaneous detection of the spin-Hall magnetoresistance and the spin-Seebeck effect in platinum and tantalum on yttrium iron garnet, *Phys. Rev. B* **90**, 174436 (2014).
- [44] T. Kikkawa, K. Uchida, S. Daimon, Z. Qiu, Y. Shiomi, and E. Saitoh, Critical suppression of spin Seebeck effect by magnetic fields, *Phys. Rev. B* **92**, 064413 (2015).
- [45] U. Ritzmann, D. Hinzke, A. Kehlberger, E.-J. Guo, M. Kläui, and U. Nowak, Magnetic field control of the spin Seebeck effect, *Phys. Rev. B* **92**, 174411 (2015).
- [46] S. T. B. Goennenwein, R. Schlitz, M. Pernpeintner, K. Ganzhorn, M. Althammer, R. Gross, and H. Huebl, Non-local magnetoresistance in YIG/Pt nanostructures, *Appl. Phys. Lett.* **107**, 172405 (2015).
- [47] L. J. Cornelissen, J. Shan, and B. J. van Wees, Temperature dependence of the magnon spin diffusion length and magnon spin conductivity in the magnetic insulator yttrium iron garnet, *Phys. Rev. B* **94**, 180402(R) (2016).
- [48] Y.-T. Chen, S. Takahashi, H. Nakayama, M. Althammer, S. T. B. Goennenwein, E. Saitoh, and G. E. W. Bauer, Theory of spin Hall magnetoresistance, *Phys. Rev. B* **87**, 144411 (2013).
- [49] L. J. Cornelissen, J. Liu, R. A. Duine, J. B. Youssef, and B. J. van Wees, Long-distance transport of magnon spin information in a magnetic insulator at room temperature, *Nat. Phys.* **11**, 1022 (2015).
- [50] J. Li, Y. Xu, M. Aldosary, C. Tang, Z. Lin, S. Zhang, R. Lake, and J. Shi, Observation of magnon-mediated current drag in Pt/Yttrium iron Garnet/Pt(Ta) trilayers, *Nat. Commun.* **7**, 10858 (2016).
- [51] H. Wu, C. H. Wan, X. Zhang, Z. H. Yuan, Q. T. Zhang, J. Y. Qin, H. X. Wei, X. F. Han, and S. Zhang, Observation of magnon-mediated electric current drag at room temperature, *Phys. Rev. B* **93**, 060403(R) (2016).